HHS Public Access

Author manuscript

Cancer Discov. Author manuscript; available in PMC 2019 September 01.

Published in final edited form as:

Cancer Discov. 2018 September ; 8(9): 1112–1129. doi:10.1158/2159-8290.CD-18-0349.

Organoid profiling identifies common responders to chemotherapy in pancreatic cancer

A full list of authors and affiliations appears at the end of the article.

Abstract

Pancreatic cancer is the most lethal common solid malignancy. Systemic therapies are often ineffective and predictive biomarkers to guide treatment are urgently needed. We generated a pancreatic cancer patient-derived organoid (PDO) library that recapitulates the mutational spectrum and transcriptional subtypes of primary pancreatic cancer. New driver oncogenes were nominated and transcriptomic analyses revealed unique clusters. PDOs exhibited heterogeneous responses to standard-of-care chemotherapeutics and investigational agents. In a case study manner, we find that PDO therapeutic profiles paralleled patient outcomes and that PDOs enable longitudinal assessment of chemo-sensitivity and evaluation of synchronous metastases. We derived organoid-based gene expression signatures of chemo-sensitivity that predicted improved responses for many patients to chemotherapy in both the adjuvant and advanced disease settings. Finally, we nominated alternative treatment strategies for chemo-refractory PDOs using targeted agent therapeutic profiling. We propose that combined molecular and therapeutic profiling of PDOs may predict clinical response and enable prospective therapeutic selection.

Keywords

Pancreatic Cancer; Organoids; Common Responders; Precision Medicine; Pharmacotyping; Pharmacotranscriptomics

Introduction

Pancreatic ductal adenocarcinoma (PDAC) is a deadly malignancy often diagnosed at advanced stages. 15 – 30% of PDAC patients are diagnosed with clinically localized disease that is amenable to potentially curative surgical resection (1, 2). Following surgical resection, the majority of patients will have local or distant recurrence (3) and succumb to the disease. Systemic treatment, in the form of neoadjuvant or adjuvant cytotoxic chemotherapy, is used in conjunction with oncologic resection but only adds a modest benefit in survival (4, 5). Most patients are not surgical candidates and are diagnosed with locally advanced or metastatic disease. Therapeutic options for these patients include the combination chemotherapy regimens Gemcitabine/nab-Paclitaxel (6) or FOLFIRINOX (5-

*Corresponding Authors: David A. Tuveson; Cold Spring Harbor Laboratory; 1 Bungtown Road; Cold Spring Harbor, NY 11724; dtuveson@cshl.edu and Steven Gallinger MD, Msc, FRCS; Toronto General Hospital; 200 Elizabeth Street; 10EN, Room 206; Toronto, Ontario; Canada M5G 2C4; steven.gallinger@uhn.ca.

[33]Equal Contribution

Conflicts of Interest: The Authors declare no conflicts of interest.

Fluorouracil, Leucovorin, Irinotecan, Oxaliplatin) (7). Despite therapeutic intervention, median overall survival is 6.7 – 11.1 months (Progression Free Survival/PFS = 3.3 – 6.4) for advanced disease (6, 7), compared to 25 – 28 months (PFS = 13.1 – 13.9) in surgically resected patients (4). Many PDAC patients have chemo-refractory disease, but a smaller subset exhibits significant response to chemotherapy. Current therapeutic selection for both local and metastatic pancreatic cancer patients is often based on patient performance status and co-morbidities. Altogether, this highlights the unmet clinical need to define responsive subgroups to inform treatment selection and to nominate alternative treatment options for patients who are resistant to currently approved treatment regimens. Therefore, approaches that predict the most effective chemotherapeutic regimen should improve patient care. To date, PDAC driver mutations have been hard to target in the clinical setting, with the exception of microsatellite instability (8), *BRCA2* mutations (9) and potentially targetable, uncommon $KRAS^{G12C}$ mutations (10). Furthermore, there are a considerable number of patients without these particular genetic alterations that would still benefit from alternative treatment strategies.

PDAC molecular subtypes have been described and validated in several independent patient cohorts (11–13). By growing consensus, two major subtypes of PDAC exist. The Basal-like, Squamous or Quasi-mesenchymal, subtype identifies PDAC patients with poor prognosis and is characterized by basal markers such as cytokeratins. The Classical or Pancreatic Progenitor subtype is characterized by differentiated ductal markers and identifies patients with a better prognosis. Moffitt and colleagues (13) found that the Classical subtype of PDAC is significantly under-represented in current PDAC cell culture models. Additional subtypes including Aberrantly Differentiated Endocrine Exocrine (ADEX) and Immunogenic subtypes have been reported (11), but The Cancer Genome Atlas pancreas cancer project recently demonstrated their association with tumors exhibiting low neoplastic cellularity, suggesting that stroma and normal pancreas contribute markedly to these subtype signatures (14). Regardless of the subtype, the low neoplastic cellularity of primary tumors makes it difficult to access molecular details regarding a particular profile of genetic alterations and gene expression changes in the neoplastic compartment.

Until recently, the phenotypic study of early and late PDAC has been hampered by a lack of tractable patient-derived models that encompass the full spectrum of disease, which would enable rapid evaluation of predictive biomarkers of treatment response. Using advances in organoid culture technology, we established the methodology to culture PDAC patient-derived organoids (PDOs) from both surgical resection specimens as well as fine needle biopsies (FNB) with a high success rate (15, 16). These cultures exhibit mutation allele frequencies indicative of pure neoplastic cultures. Seino and colleagues have generated and characterized a library of 39 PDO cultures (17), which recapitulate the expected DNA signature of PDAC and exhibit a differential Wnt dependence that was inversely correlated with the Classical subtype. However, the utility of pancreatic cancer PDO cultures for defining predictive biomarkers of treatment response remains to be explored.

Herein we describe a library of 66 PDO cultures obtained from fine needle biopsy, surgical resection, and rapid autopsy PDAC specimens collected from multiple clinical institutions. Using deep molecular characterization of the PDO genome and transcriptome, we identify

the expected hallmarks of PDAC. In addition, we find high concordance between the primary tumor and paired PDO samples when sufficient neoplastic cellularity was observed in the patient specimen. We establish a PDAC-specific PDO drug-testing pipeline, termed “pharmacotyping”, and demonstrate that drug sensitivity profiles can be generated for each PDO within a clinically meaningful timeframe. In a retrospective analysis of a small subset of advanced PDAC patients from whom the PDOs were generated, the PDO chemotherapy sensitivity profile reflected patient response to therapy. These studies suggest that drug testing in PDO cultures may be used to inform treatment selection. In addition, longitudinal sampling in a single patient predicted acquisition of resistance to chemotherapy that paralleled clinical disease progression. Furthermore, several PDO cultures resistant to all available chemotherapeutic options exhibited exceptional sensitivity to targeted agents, providing alternative treatment options for chemo-refractory disease. Finally, to identify patients most likely to benefit from chemotherapy, we generated PDO-derived gene signatures predictive of chemotherapy sensitivity. We demonstrate that these chemo-sensitivity signatures can retrospectively identify large groups of PDAC patients who are more likely to respond to several chemotherapeutics in either the adjuvant or advanced disease settings. These chemo-sensitivity signatures may enable more rapid treatment stratification of PDAC patients into those that may benefit from currently available chemotherapeutic interventions and those that should instead be considered for rationally targeted and investigational agents.

Results

Assembling a pancreatic cancer patient-derived organoid library

Previously, tumor models of patients with metastatic PDAC were often difficult to generate because of the limited material available from diagnostic biopsies. To comprehensively model the full clinical spectrum of PDAC, we obtained 159 human samples from primary tumors (hT) and metastases (hM) in 138 patients for PDO generation (15, 17) (Figure S1). Seventy-eight (78) specimens were isolated from surgical resections, 60 from fine needle biopsies of primary or metastatic lesions (hF), 20 from metastatic disease following rapid autopsies and 1 from a video-assisted thoracoscopic surgical (VATS) resection of a lung metastasis. Organoid culture conditions do not enable the survival or outgrowth of non-epithelial cells (15). We successfully generated PDO cultures that expanded for at least 5 passages. Using these metrics, the PDO generation efficiency was 75% (72% for fine needle biopsies - hF, 78% for tumor resections - hT), resulting in a total of 114 PDO cultures from 101 patients (73% of patients) (Figure 1A). As previously reported by Seino and colleagues, addition of serum to the culture media was detrimental to the isolation and propagation efficiency (17). The pancreatic cancer PDOs exhibited mixed morphology consisting of hollow epithelial lined cystic structures with differing degrees of filled lumens (Figure 1B). In parallel, 11 human normal (hN) pancreatic ductal organoids were established from heathy normal pancreata obtained from islet transplant centers (15, 17) (Table S1A), all of which exhibited a hollow epithelial cystic architecture.

Patient-derived organoids recapitulate genetic hallmarks of pancreatic cancer and reveal new characteristics

We developed a precision medicine pipeline that first focuses on molecular characterization of the PDO library as the organoid cultures pass quality control criteria (Figure S1). The criteria to be classified as a confirmed tumor PDO culture required the presence of known pathogenic mutations. Eighty-eight (88) PDO cultures have thus far been subjected to Sanger (*KRAS* only) or whole exome sequencing (WES), and 69 (78%) of the PDO cultures harbored genetic alterations consistent with PDAC (Figures 1C–D, S1, Table S1A–D). Nineteen (19, 22%) PDOs exhibited diploid genomes without discernable genetic hallmarks of pancreatic cancer, suggesting the outgrowth of normal ductal epithelial cells as previously reported (17), and were not further analyzed. The 11 hN organoid cultures isolated from the exocrine compartment obtained from normal healthy donors for islet cell transplantation were also subjected to WES and maintained a diploid genome without *bona fide* pathogenic mutations (Figure 1C–D). De-identified patient clinical data were available for the 69 confirmed PDAC PDO cultures. 12 PDAC PDO cultures were generated from 5 pre-treated patients with metastatic disease while the remaining 57 organoids were isolated from 55 patients who were treatment naïve at the time of PDO generation. Given that many patients who present with resectable disease typically receive neo-adjuvant therapy prior to surgical resection, this PDO library is a unique resource. For 66 of the PDAC patients with clinical stage data, PDO cultures were generated from patients with stage 1 (n = 1), 2 (n = 34), 3 (n = 7) and 4 (n = 24) disease (Table S1A).

KRAS was mutated in 66/69 PDOs (96%), while 3/69 organoids presented with wildtype *KRAS*. The expected prevalence of *KRAS* mutations was observed in the PDO cultures, with 31 (45%) cases exhibiting G12V, 29 (42%) G12D, 4 (6%) G12R, 2 (3%) Q61H, and 3 (4%) wildtype *KRAS*. In 2 (3%) cases, multiple *KRAS* mutations were detected within a single PDO culture (Table S1A), with one case exhibiting a bi-allelic $KRAS^{G12V}$ and $KRAS^{G12R}$ mutation (hF50) and the other (hF70) exhibiting an amplified KRAS allele likely harboring a compound $KRAS^{G12D,G179S}$ mutation. Of the *KRAS* wildtype PDO cultures, hF43 harbored an oncogenic $PIK3CA^{E110del}$ allele (18), hF39 exhibited an activating $MAP2K1^{Q58\_E62del}$ allele associated with MEK1 inhibitor resistance (19, 20), and hT102 harbored a hyper-activating mutation of $ERBB2^{S310F}$ (21) concomitant with a copy number gain of the wildtype *ERBB2* allele. *TP53* mutations were detected in 58/66 (88%) of the organoids subjected to WES (excluding the *KRAS* only Sanger Sequenced organoids) and were concomitant with loss of heterozygosity (LOH) in 56/58 cases (97%) (Table S1B). In addition, we observed a high rate of deep copy number loss ($\log_2 < -3$) or homozygous, inactivating mutation of *CDKN2A* (n = 32% and 24%, respectively) and *SMAD4* (n = 8% and 20%, respectively). 35% of *KRAS* mutant PDO cultures exhibited inactivation of all three commonly altered PDAC tumor suppressor genes (*TP53*, *SMAD4*, *CDKN2A*) while 45% exhibited inactivation of two of these tumor suppressors (Table S1C). A small fraction (14%) of the *KRAS* mutant PDOs harbored inactivation of only one tumor suppressor. 64 out of the 66 PDAC PDO cultures subjected to WES were aneuploid, while two cultures, hT83 and hF43, maintained a largely diploid genome (Figure S2A). For these cultures, hT83 harbored a $KRAS^{G12R}$ and *TP53* mutation, but did not exhibit *TP53* LOH or inactivation of other canonical tumor suppressor genes; whereas hF43 had features of mismatch repair

deficiency, including *MSH6* mutation, complete loss of *MLH1* and a frequency of insertions and deletions (per megabase) more than 8-fold higher than the cohort mean (11.54 versus 1.303 indels/MB) (Fig. S2B) (22).

Whole genome sequencing (WGS) was performed on a subset of PDAC-confirmed PDOs derived from surgical resections and their matched primary tumor (bulk), and both were germline corrected using normal tissue (n = 13) (Figure 2A, S2C). 82.49% – 99.96% (mean 97.43%) of the mutations detected in the primary tumor specimen were also detected in the PDO culture. The four most commonly altered genes in PDAC (*KRAS, TP53, CDKN2A, SMAD4*) were also examined for their overlap between matched primary and PDO specimens. In 11 of the 13 cases, the PDO cultures completely recapitulated the PDAC core mutation profile found in the patient, although in the primary tumor specimens, there were often low numbers of reads and the mutation was not confidently called (Table S1D). The primary tumor specimens from the two sample pairs that did not exhibit overlap had extremely low purity (<15%) and no alterations in PDAC core genes were detected in the primary tumor specimens. High concordance of somatic mutations was achieved between the primary tumor and PDO in most cases (6 > 80%, 11 > 59%), with more somatic mutations detected in the PDO cultures due to the pauci-cellular nature of the primary tumors and high neoplastic purity of the organoids. In 2 cases where there was low tumor purity (<15%), low concordance (<10%) was observed, likely due to the limited ability to detect somatic mutations in the pauci-cellular primary tumors compared to the increased ability to extract genetic alterations from the purely neoplastic PDO cultures. Copy number analyses of the paired primary tumors and PDOs also showed concordance in the primary specimen with high purity (purity > 40%, hT98) (Figure 2B), however, most primary tumor specimens had insufficient purity to reveal copy number alterations (CNA), whereas CNA and gross chromosomal rearrangements were readily discernable in the PDO cultures (Figures 2C, S2D, S3). In addition to the hT PDO and primary tumor pairings, WGS with germline correction was also performed on 8 hF PDO cultures. Due to the small amount of tissue obtained from these biopsies, the entire specimen was directed towards PDO generation such that primary tumor tissue from the hF PDO cultures was unavailable for comparison. Complex genomic rearrangements were also observed in several of the PDO hF cultures (Figures S3). While genetic assessment of PDAC primary tissue specimens is often challenging due to their low neoplastic cellularity, these genomic analyses revealed the high depth and clarity in which PDAC genetics can be evaluated in PDO cultures, providing alternative means of identifying actionable genetic alterations in PDAC patients.

Transcriptomic profiling and subtyping of pancreatic cancer PDO cultures

RNA sequencing was performed on 44 PDAC-confirmed PDOs and 11 hN organoid cultures. The hN cultures clustered separately from the PDAC PDOs in principal component analysis (Figure 3A). The hM19A-D series of organoids were isolated from different metastatic sites of the same patient following rapid autopsy and represent a distinct cluster relative to the other stage 4 PDO cultures. Gene set enrichment analysis (GSEA) of the differentially expressed genes in PDAC relative to hN organoids indicated an enrichment in MYC and E2F targets, the G2M Checkpoint, as well as pathways involved in metabolism that include glutathione metabolism, steroid biosynthesis, and biosynthesis of unsaturated

fatty acids (Table S2). These PDO RNA sequencing data were used to identify the Classical and Basal-like subtype signatures previously derived from bulk tissues following virtual microdissection (13) (Figure 3B). 70% of the PDO cultures are the Classical subtype (31/44) and 30% are Basal-like (13/44) - a notable finding as there are very few available cell line models of the Classical PDAC subtype (13) (Table S3A). Therefore, in addition to being able to efficiently culture organoids from every stage of pancreatic cancer, including previously difficult to access metastatic disease, this culture method enables the propagation and study of PDO cultures from both Classical and Basal-like PDAC subtypes.

The PDO transcriptomes were also independently classified using non-negative matrix factorization (NMF) clustering, revealing two stable clusters in PDAC PDO cultures (Figure 3C, S4A–B and Table S3B). Cluster C1 was enriched for TGFβ signaling and EMT by GSEA (Figure 3D, Table S2). In contrast, Cluster C2 exhibited enrichment for xenobiotic metabolism, fatty acid metabolism, and oxidative phosphorylation by GSEA. While the genes comprising the C1/C2 signatures did not overlap with those defining Basal and Classical subtypes (1 gene overlap is *MYO1A*), the classifications were largely concordant with 83% of the Basal-like PDO cultures falling in the C1 classifier and 93% of the Classical PDO cultures falling in the C2 cluster. Therefore, PDO cultures revealed unique gene expression programs that divide PDAC into two distinct molecular classes.

PDO pharmacotyping corresponds with individual patient treatment responses

Therapeutic profiling or “pharmacotyping” was performed on 66 PDAC-confirmed PDOs using the five chemotherapeutic agents most commonly used to treat PDAC patients: Gemcitabine, nab-Paclitaxel (Paclitaxel used in PDOs), Irinotecan (SN-38, active metabolite used in PDOs), 5-Fluorouracil (5-FU) and Oxaliplatin. PDO pharmacotyping revealed marked interpatient variability in the PDO response to single chemotherapy agents as evaluated using dose response curves and the corresponding area under the curves (AUC) (Figure 4A–E, Table S4A). The PDO culture pharmacotyping was stable over multiple passages with minor variation only occasionally observed (Figure S5). For each chemotherapeutic agent, we divided the PDO library into three subgroups: the least responsive (resistant, top 34% AUC), the most responsive (sensitive, lowest 33% AUC) and those exhibiting intermediate response (middle 33% AUC). To determine whether this subgrouping was informative for individual patients, we obtained retrospective clinical follow-up from 9 patients with advanced PDAC who were treated with these 5 agents (Figure S6A). Of the 6 patients with a progression-free survival (PFS) longer than the published median PFS (6, 7), 5 were treated with at least one drug to which the matched PDO culture was particularly sensitive and no drug to which the matched PDO culture was resistant. These 6 patients had a mean PFS of 332 days compared to the expected PFS of 180 days (6, 7). Two (2) of the 3 patients who rapidly progressed were treated with a chemotherapeutic agent to which their PDO was markedly resistant. One of the nine patients exhibited an outcome inconsistent with the matched PDO (hF50) pharmacotyping profile. Altogether, these data suggest the potential relevance of this approach.

For one patient, corresponding with PDO hF2, extensive retrospective data was available following the generation of the PDO. The PDAC patient from which the hF2 PDO was

generated was first treated with a four-drug combination including two drugs with an intermediate PDO response profile (Oxaliplatin and 5-FU) and one drug with a resistant PDO response (Paclitaxel) (Figure S6B–C). This patient exhibited early progression in both the primary and metastatic sites (Figure S6C) and was switched to a second line regimen that contained two drugs to which the PDO was sensitive (Gemcitabine and SN-38). Following the change in regimen, the patient exhibited a partial response for 388 days before adopting third and fourth line therapeutic strategies until ultimately succumbing to disease 1,020 days following diagnosis (Figure S6C). For this single patient case study, the retrospective clinical data paralleled the PDO chemo-sensitivity profile.

Temporal evolution of PDO chemo-sensitivity

In an analogous case study manner, we found that longitudinal PDO generation reflected the clinical course for an individual patient (Figure 5A). In the hM1 series, the hM1A PDO was isolated from a VATS resection of a lung metastasis and following resection the patient was found to respond well to both FOLFIRINOX and Gemcitabine/nab-Paclitaxel regimens. Indeed, the hM1A PDO was sensitive to Gemcitabine, Paclitaxel, 5-FU and Oxaliplatin and exhibited an intermediate SN-38 response within our cohort. Approximately two years later, the patient presented with progressive disease that histologically exhibited neuroendocrine/small cell-like characteristics. A repeat organoid culture, hM1E, was established from a percutaneous core biopsy of a lung metastasis. The patient succumbed to the disease shortly afterwards and a rapid autopsy was performed, leading to the generation of the final hM1F organoid. Intriguingly, the hM1E and hM1F PDO cultures showed amplification of the *KRAS* allele (Figure 1D) and were resistant to Gemcitabine, Paclitaxel, and SN-38 while hM1F gained additional resistance to Oxaliplatin and switched to a more Basal-like subtype (Figure 3B). This case suggests the utility of longitudinal PDO sampling following repeat biopsies to evaluate the acquisition of resistance mechanisms to first line chemotherapeutic regimens. At the same time, this longitudinal case series revealed resistance to all commonly used chemotherapeutics for pancreatic cancer, a common issue observed in several PDO cultures and encountered in the clinic.

Spatial intra-patient heterogeneity of chemo-sensitivity

We also examined the therapeutic sensitivity of four different PDO cultures generated from two liver (hM19A, B) and one diaphragmatic metastases (hM19C), as well as ascites (hM19D) from the same patient following a rapid autopsy (Figure 5B). We found that these four hM19 cultures exhibited similar therapeutic profiles to three chemotherapeutic agents, but different sensitivities to 5-FU. While these four PDOs harbored similar DNA mutations by exomic sequencing (Figure 1C), they possessed small differences in CNA (Figure 1D) and mRNA expression (Figure 3A–C). Whether these molecular differences underlie this therapeutic profile heterogeneity remains to be determined, and this case highlights the possibility that metastatic patients may possess different cancer subclones that will require novel therapeutic regimens to achieve the best clinical response.

Nomination of alternative treatment strategies for chemo-refractory PDO cultures

To ascertain alternative treatment strategies for PDO cultures, pharmacotyping was performed using a panel of targeted agents (n = 21) on 66 PDAC-confirmed PDO cultures

(Figure S7A, Table S4B). Among the PDO cultures lacking sensitivity to any of the five chemotherapeutic agents (n = 22 out of 66, 33%) (Table S4C), alternative treatment strategies were evaluated for 21 of these PDO cultures. We were able to identify targeted agents with extreme PDO sensitivity (10% most sensitive) for half (n = 11) of these chemotherapy-insensitive PDO cultures. For example, hT89 was resistant to four chemotherapeutic regimens, but sensitive to the broad-spectrum kinase inhibitor Sunitinib (Table S4C). Targeted agent sensitivities were also evaluated for chemo-sensitive PDO cultures. For instance, hT105, which was sensitive to Oxaliplatin and Paclitaxel, was also sensitive to several targeted agents including Selumetinib, Afatinib, Everolimus and LY2874455 (FGFR inhibitor). In line with previous findings, the PDO hF39 that harbors the oncogenic MEK1 allele *MAP2K1*$^{Q58\_E62del}$ was not sensitive to MEK inhibitor Selumetinib (20). The ERBB-directed agent Afatinib showed increased activity towards PDOs harboring *ERBB2* amplification, with the most sensitive PDO being the *KRAS* wildtype PDO hT102 that harbors the hyper-activating *ERBB2*^{S310F} allele in the setting of amplifications in *EGFR*, *ERBB2* and *AKT2* (Figure 5C). Evaluation of other genes involved with homologous repair deficiency revealed that while there are many haploid losses in the copy number of these genes, these single copy losses do not correspond with Olaparib sensitivity (Figure 5D, 1D, S7B). Deleterious *BRCA1/2* mutations were not present in this PDO library. Nonetheless, a trend was observed between Olaparib sensitivity and complete loss of *PALB2* (Figure 1C–D). The only organoid harboring a *PIK3CA* mutation, the *KRAS* wildtype PDO hF43 that carried the oncogenic *PIK3CA*^{E110del} allele (18), was highly sensitive to the Rapamycin analogue Everolimus (Figure 5E). Finally, the previously mentioned hM1 longitudinal series includes hM1A, which was isolated from a lung metastasis and exhibited a pancreatic ductal adenocarcinoma pathology while the two PDO cultures, hM1E and hM1F were isolated after the lung metastases switched to a small cell-like (neuroendocrine) phenotype. Neuroendocrine tumors are often responsive to mTOR inhibition (24), which is potentially paralleled by the switch of the hM1 series from an average to a sensitive Everolimus therapeutic profile (Figure 5E). These results suggest that targeted therapy sensitivities empirically identified in PDO pharmacotyping may supplement precision medicine approaches for PDAC patients.

PDO pharmacotranscriptomic signature reflects treatment response in pancreatic cancer patients

To investigate whether PDO pharmacotyping could be applied to advanced pancreatic cancer patients, we generated drug sensitivity signatures by correlating PDO transcriptional profiles with the pharmacotyping results. For each chemotherapeutic agent, we computed the Spearman correlation between PDO gene expression and the AUC for each drug, and thereby defined distinct transcriptional signatures (Figures 6A, S8, S9A–E, S10A–B and Table S5A–E). We refined the signatures to include genes that increased in expression when AUC decreased (negative rho value), which is indicative of increased drug sensitivity. By clustering the PDO cultures using the individual drug response signatures, the PDOs could be grouped into sensitive or non-sensitive classes for each individual chemotherapeutic signature. To determine whether the PDO-derived pharmacotranscriptomic signatures reflected treatment responses in patients, we obtained neoplastic cell-enriched gene expression data and associated clinical details from 126 patients who underwent resection of

their pancreatic tumor and then either received adjuvant treatment (n = 95) or no treatment (n = 31) (ICGC-CA) (25). In this sample set, 43% of the patient tumors (55/126) were the Basal-like subtype of PDAC. Treated patients received either Gemcitabine alone or in combination with other chemotherapeutic agents. Therefore, we applied the Gemcitabine-specific PDO sensitivity signature to this patient cohort and determined that 50% of patients were enriched (Figure S11A). We used this signature to evaluate patient response in the subgroup of 55 patients who received Gemcitabine monotherapy, and found that patients with enrichment for the Gemcitabine sensitivity signature had a significantly better progression free survival (PFS, 772 vs 373 days, HR= 0.54, $P = 0.04$) (Figure 6B–C), and a trend towards improved overall survival (OS) (Figure S11B). Interestingly, in this cohort of 55 patients, the Basal-like subtype was similarly represented in the Gemcitabine sensitive and non-sensitive groups (Figure 6B). Application of this gemcitabine sensitivity transcriptomic signature to a larger subgroup of 91 patients who either received Gemcitabine monotherapy or Gemcitabine in combination with 5-FU or Cisplatin also identified patients with a significantly better PFS, but not OS (Figure S11C–D). In the small cohort of 30 untreated patients, the Gemcitabine sensitivity signature did not identify patients with improved PFS or OS, demonstrating that this signature is treatment dependent (Figure 6D, S11E–F).

Finally, the chemo-sensitivity signatures were applied to an independent transcriptomic data set obtained from tumors of PDAC patients on the COMPASS trial (26). Patients on the COMPASS trial had advanced pancreatic cancer and underwent core needle biopsy prior to treatment with combination chemotherapy. The biopsies were of sufficient size to perform laser capture micro-dissection for mRNA isolation and transcriptomic analysis. 30% of the tumors (22/73) were the Basal-like subtype of PDAC. We found that 44, 37, 31, 29 and 36 (60%, 51%, 42%, 40% and 49%) patients exhibited enrichment for the PDO-derived sensitivity signatures for Oxaliplatin, 5-FU, SN-38, Gemcitabine and Paclitaxel, respectively (Figure 7A, S12A–D). The Basal-like patients were equally distributed between the chemo-sensitive and non-sensitive signatures with the exception of Oxaliplatin, which exhibited an enrichment of the Basal-like subtype in the non-sensitive patient group (Figure 7A, S12A–D). Response evaluation criteria in solid tumors (RECIST) measurements were available for most patients 8 weeks following the initiation of therapy. We found that the Oxaliplatin signature significantly correlated with response ($r = -0.396$, $P = 0.0078$) in patients receiving FOLFIRINOX (n = 47). Patients that had an enrichment for the Oxaliplatin signature exhibited better tumor responses to FOLFIRINOX than their non-sensitive counterparts, but the 5-FU and SN-38 signatures did not provide additional information (Figure 7B). There was also a trend for increased overall survival in the Oxaliplatin sensitive patients (Figure 7C), and notably there is a larger number of patients still alive in the Oxaliplatin sensitive (n = 13) versus non-sensitive cohorts (n = 5). Intriguingly, of the 6 Basal-like patients that lacked enrichment of the Oxaliplatin chemo-sensitivity signature and progressed on FOLFIRINOX, 5 exhibited enrichment for the Gemcitabine chemo-sensitivity signature (Figure 7B).

19 tumor biopsies from patients with advanced PDAC were obtained prior to treatment with the combination chemotherapy regimen Gemcitabine and nab-Paclitaxel, and RECIST criteria was again measured at 8 weeks. In this smaller subset of patients, 7 patients harbored

the Gemcitabine sensitivity signature and 7 patients also exhibited the Paclitaxel sensitivity signature (Figure S12A–B, S13). The 4 patients that were sensitive to both Gemcitabine and Paclitaxel had reduced tumor sizes by their 8-week radiological evaluation and many patients sensitive to either Gemcitabine or Paclitaxel also responded, although the sample size is limited and the analysis interim (Figure S13). The ability of the PDO chemo-sensitivity signatures to expediently identify patients with better response in both the ICGC-CA and COMPASS studies suggest that these signatures may have potential clinical utility following evaluation in prospective clinical trials.

Discussion

The poor response of PDAC patients to therapies has been attributed to neoplastic cell characteristics such as cancer stem cells (17), redox metabolism (27) and intermediary metabolism (28, 29); and to non-cell autonomous properties such as limited drug delivery (30–32), impaired intra-tumoral immunity (33) and fibroblast- and microbial-mediated drug metabolism (34, 35). While the influence of different matrix components or cancer-associated fibroblasts to therapeutic response is worthy of future examination, in this study, we employ PDOs as a well-defined model system and demonstrate a broad range of intrinsic neoplastic cell drug sensitivities to conventional chemotherapeutic agents. These data reveal the additional impact of interpatient diversity to chemotherapeutic drug responses that may supersede or modify other potential causes of drug resistance. The biological basis of this interpatient drug responsiveness is currently under investigation and may involve drug transport, metabolism and/or response to cell damage. Importantly, such questions may be addressed with PDOs as they are representative of the various features of PDAC observed across a large population, including a similar distribution of the Basal-like and Classical PDAC subtypes: 30% compared to 70%, respectively. By considering individual drug sensitivities in organoids, transcriptional signatures were derived that mirrored patient outcomes in two separate clinical cohorts following the adjuvant treatment of patients with Gemcitabine, or the palliative treatment of patients with modified-FOLFIRINOX or Gemcitabine/nAb-Paclitaxel. These signatures may identify common responders to first line chemotherapy agents and enable stratification of patients such that they may rapidly achieve clinical benefits while more tailored treatments can be developed for each patient. Interestingly, there are a number of patients who exhibit enrichment for the chemo-sensitivity signatures in both the adjuvant and the advanced disease setting that are continuing to respond. Whether these long-term surviving, chemo-sensitive patients represent exceptional responders to either Gemcitabine or Oxaliplatin will require additional investigation. The 5-FU sensitivity signature, which contained a relatively small number of genes, did not perform well when evaluated in patients and will require further laboratory assessment and optimization. Additionally, while promising in PDOs, the SN-38 signature did not clarify the impact of the Oxaliplatin signature in the COMPASS trial patients. This may reflect the reduced Irinotecan dosing on the modified FOLFIRINOX regimen and/or the need to further refine the SN-38 signature. On the other hand, the Gemcitabine, Oxaliplatin and Paclitaxel signatures show concordance with patient responses in our preliminary studies. Cases that lack concordance with the Oxaliplatin, Gemcitabine and Paclitaxel chemo-sensitivity signatures may represent intra-tumoral heterogeneity that existed at the

initiation of therapy or evolved quickly. Methods that utilize non-invasive biomarkers as surrogates for disease response may facilitate rapid adjustment to a more effective therapeutic regiment for patients. Additionally, while both subtypes of pancreatic cancer were found in the chemo-sensitive and non-sensitive transcriptomic subgroups, there was enrichment for the Basal-like subtype in the Oxaliplatin non-sensitive group. Of note, some of these Oxaliplatin non-sensitive patients demonstrated enrichment for other chemo-sensitivity signatures, suggesting that alternative chemotherapies might be beneficial to those patients. Going forward, these pharmacotranscriptomic signatures will need to be refined and prospectively evaluated on larger cohorts of patients from whom high-quality PDAC transcriptomes can be obtained.

While the pharmacotranscriptomic signatures can conceivably immediately benefit many PDAC patients, an additional group of patients may also benefit from organoid profiling with investigational agents that are available in a clinical trial setting. Indeed, approximately one third of the PDAC PDOs lacked sensitivity to any of the five chemotherapies evaluated. For these chemotherapy non-sensitive PDOs, 52% (11 out of 21) of the PDO cultures demonstrated sensitivity to one or several targeted agents on the small panel we employed. Whether these PDO sensitivities will translate into clinical responses in patients has yet to be determined in prospective clinical trials. Additionally, our study has focused on assessing single agent activity, and it is likely that drug combinations may yield more clinical opportunities in the future.

Low cellularity is a common problem in primary pancreatic cancer specimens, often making it difficult to discern molecular characteristics with high clarity and depth. Indeed, we found few genetic alterations when assessing primary tumor specimens in all but 1 out of 13 cases that were analyzed by WGS. In contrast, the PDO cultures yielded mutations with the expected allele frequency for pure, neoplastic cultures in addition to complex genetic rearrangements. These analyses and the high concordance between primary tumor specimens and their associated PDO cultures demonstrate the added benefit of performing deep genetic analyses on PDO cultures. In addition to thoroughly characterizing the canonical genomic hallmarks of pancreatic cancer, three cases of *KRAS* wildtype pancreatic cancer were identified that harbored uncommon oncogenic drivers such as the oncogenic alleles *ERBB2*^{S310F}, *MAP2K1*$^{Q58\text{-}E62del}$ and *PIK3CA*^{E110del}. In two of these cases, exquisite sensitivities to Afatinib (*ERBB2*^{S310F}, hT102) and Everolimus (*PIK3CA*^{E110del}, hF43) were observed, suggesting that these are actionable genetic alterations.

Precision medicine approaches for pancreatic cancer are challenging due to the short median survival of metastatic pancreatic cancer patients. In some cases, PDO pharmacotyping was completed in less than 6 weeks, demonstrating the ability of the PDO pharmacotyping to produce recommendations within a clinically meaningful timeframe for both early and late stage pancreatic cancer. Complementary genomic and transcriptomic profiling has recently been shown to be feasible for advanced pancreatic cancer patients (26), thus providing further capacity to validate PDO phamacotyping and pharmacotranscriptomic signatures in a prospective manner, even when first-line therapy is being selected. The technology of generating and analyzing PDOs will continue to iteratively improve as the methodology is not uniformly successful for all patients. Altogether, these early results suggest that chemo-

sensitivity signatures may stratify and thereby improve the initial care of pancreatic cancer patients. Furthermore, when coupled with longitudinal PDO molecular and pharmacological profiling, this approach can be tailored to optimize the care of individual patients. This strategy should not be limited to pancreatic cancer.

Conclusion

We generated a pancreatic cancer, patient-derived organoid library that encompasses a broad spectrum of disease stage, uncommon genetic events as well as the previously established subtypes of pancreatic cancer. PDO cultures facilitate in depth molecular characterization that has been traditionally challenging in the unique pauci-cellular state of primary pancreatic tumors. PDO profiling using next-generation sequencing of DNA and RNA combined with pharmacotyping may predict responses in pancreatic cancer patients and provide a rational for prioritizing therapeutic regimens. This approach merits further evaluation in prospective clinical trials for pancreatic cancer patients.

Methods

Human specimens

Normal pancreatic tissues were obtained from the islet transplant program at the University of Miami Miller School of Medicine as described previously (15). Pancreatic cancer tissue was obtained from patients undergoing surgical resection or tissue biopsy at Memorial Sloan Kettering, Stony Brook University (GI Cancer Clinical Resource Core), Johns Hopkins University, Northwell Health, Weill Cornell University, University of California Davis, and Thomas Jefferson University Hospital, MD Anderson Cancer Center, Washington University St. Louis, and St. Francis hospital. Autopsy specimens from metastatic sites were obtained from Rapid Autopsy Program at University of Nebraska Medical Center and Washington University St. Louis. All tissue donations and experiments were reviewed and approved by the Institutional Review Board of Cold Spring Harbor Laboratory and all clinical institutions. Written informed consent was obtained prior to acquisition of tissue from all patients. The studies were conducted in accordance to recognized ethical guidelines (Declaration of Helsinki). Samples were confirmed to be tumor or normal based on pathologist assessment.

Organoids, cell cultures and culture conditions

For human samples, tissues were minced and incubated in digestion media (1mg/mL Collagenase XI, 10μg/mL DNAse I, 10.5μM Y-27632 in Human complete Medium) at 37˚C with mild agitation for up to 1 hour. Cells were plated with Matrigel and grown in Human complete Feeding Medium: advanced DMEM/F12, HEPES 10mM, Glutamax 1X, A83-01 500nM, hEGF 50ng/mL, mNoggin 100ng/mL, hFGF10 100ng/mL, hGastrin I 0.01μM, N-acetylcysteine 1.25mM, Nicotinamide 10mM, PGE2 1μM, B27 supplement 1X final, R-spondin1 conditioned media 10% final, Afamin/Wnt3A conditioned media 50% final (17, 36). Organoid nomenclature is as follows: human normal (hN), human tumor obtained from resections (hT), human fine needle biopsies obtained by either fine needle aspiration or by core biopsy (hF), and human metastasis obtained from direct resection of metastases

following rapid autopsy or VATS resection (hM). All organoid models were isolated, cultured, and routinely tested for Mycoplasma at Cold Spring Harbor Laboratory. Organoid models were characterized by DNA sequencing, and no additional authentication was performed.

WGS library preparation and sequencing

Whole genome sequencing (WGS) libraries were prepared using the Truseq DNA PCR-free Library Preparation Kit in accordance with the manufacturer's instructions. Briefly, 1ug of DNA was sheared using a Covaris LE220 sonicator (adaptive focused acoustics). DNA fragments underwent bead-based size selection and were subsequently end-repaired, adenylated, and ligated to Illumina sequencing adapters. Final libraries were evaluated using fluorescent-based assays including qPCR with the Universal KAPA Library Quantification Kit and Fragment Analyzer (Advanced Analytics) or BioAnalyzer (Agilent 2100). Libraries were sequenced on an Illumina HiSeq X sequencer (v2.5 chemistry) using 2 x 150bp cycles aiming for 40, 60, and 80X coverage for normal germline, PDO, and primary tumor specimens.

Exome panel library preparation and sequencing

Whole exome sequencing (WES) libraries were prepared using the KAPA Hyper Prep (Roche) and xGen Research Exome v1 Panel probes (Integrated DNA Technologies) in accordance with the manufacturer's instructions. Briefly, 200ng of DNA was sheared using a Covaris LE220 sonicator (adaptive focused acoustics). DNA fragments were end-repaired, adenylated, ligated to Illumina sequencing adapters, amplified 7 cycles. The libraries were normalized and pooled equal molar in 12-plex ponds. A total mass of 2500ng of the pre-capture ponds were blocked and hybridized for 16 hours with the probes following the manufacturer's recommendations. Resulting captured libraries were then amplified 10 cycles. Final libraries were evaluated using fluorescent-based assays including PicoGreen (Life Technologies) and Fragment Analyzer (Advanced Analytics) and they were sequenced on an Illumina HiSeq2500 sequencer (v4 chemistry) using 2 x 125bp cycles aiming for 50X coverage.

Sequencing Pre-Processing and Variant Calling

WGS and WES data for the tumor, organoid and matched normal samples were processed by the NYGC somatic pre-processing pipeline which includes aligning reads to the GRCh37 human reference genome using the Burrows-Wheeler Aligner (BWA) (37), marking of duplicate reads by the use of NovoSort (a multi-threaded bam sort/merge tool by Novocraft technologies http://www.novocraft.com), joint indel realignment for matched samples, and base recalibration via Genome Analysis Toolkit (GATK) (38). The Exome study used the HapMap NA12878 sample in place of a matched normal sample, which was processed using the same protocol as the organoid samples. Somatic Single Nucleotide Variant (SNV) calling is performed using muTect v1.1.7 (39), LoFreq v2.1.3a (40), and Strelka v1.0.14 (41), and indel calling was performed using Pindel v0.2.5 (42), Scalpel v0.5.3 (43) and Strelka v1.0.14. Structural nucleotide variants (SNVs) were detected by the use of Crest v1.0 (44), Delly v0.6.1 (45), and BreakDancer v1.4.0 (46). Copy-number variants (CNVs) were detected using NBIC-seq v0.7 (47) for WGS, and FACETS v0.5.2 (48) for Exome, resulting

in segmented profiles where the copy number is approximated by a piecewise-constant function of the genomic position.

Organoid-Tumor SNV Concordance

SNV concordance between tumor-organoid pairs was determined from the overlap of variant calls and variant allelic fractions. For each SNV called in the tumor or organoid, we ran Samtools Pileup (with minimum base quality and minimum mapping quality of 10) at this position for both samples to compute the variant allele fractions. If read evidence for the SNV was present in both samples (and therefore VAF>0), the SNV was considered concordant. To add confidence to this analysis, we only included SNVs that were called by 2 or more variant callers in at least one of the samples.

Organoid-Tumor CNV Comparison

CNVs were compared between organoids and tumors by plotting the CNV $\log_2$ values across chromosomes. A threshold of −0.235 and 0.2 was used to delineate the cutoff for deletions and amplifications, respectively. This threshold is based off of a diploid sample with 30% purity. Neutral segments are colored in green, and deletions/amplifications in red. The y-axis range is smaller for the tumor samples so that possible CNVs can be more easily identified.

WGS Purity / Ploidy Estimates

Purity and ploidy for each sample was manually calculated by comparing the VAF of somatic SNV, BAF, and CNV $\log_2$ values of multiple variants within each sample. The final average ploidy/purity was taken from the Titan (49) or ABSOLUTE (50) estimate that most closely matched the manual calculation. No exact purity estimates were made for tumor samples that seem to have extremely low purity (<15%).

SNV and CNV landscape visualization

The SNV landscape is displayed using the Bioconductor package GenVisR v1.8.0 (51). The CNV per gene heatmap was generated using the Bioconductor package ComplexHeatmap v1.17.1 (52). A $\log_2$ value was assigned to each gene using the CNV region that covered at least 50% of the gene via a custom R script. When no CNV region respected that threshold, the gene was assigned a “No information” label. The CNV landscape per chromosome was illustrated using Bioconductor package gtrellis v1.11.1 (53).

RNA-sequencing library construction

For RNA-sequencing experiments, organoids in matrigel were lysed directly with 1 mL of TRIzol reagent (Thermo Fisher) and total RNA was extracted according to the manufacturer’s instructions. RNA-seq libraries were constructed using the TruSeq sample Prep Kit V2 (Illumina) according to the manufacturer’s instructions. Briefly, 2μg of purified RNA was poly-A selected and fragmented with fragmentation enzyme. cDNA was synthesized with Super Script II master mix, followed by end repair, A-tailing and PCR amplification. RNA-seq libraries were sequenced using an Illumina HiSeq2500 or NextSeq

platform with paired-end reads of 125 bases (Cold Spring Harbor Genome Center, Woodbury).

RNA-seq analysis

RNA-seq reads quality was first quantified using FastQC v0.11.5 [https://www.bioinformatics.babraham.ac.uk/projects/fastqc]. Reads were then trimmed using Trimmomatic v0.36 (54) and aligned using STAR v2.5.2b (55) on the transcripts corresponding to the human genome (GRCh38.p10 assembly) and obtained from GENCODE (release 27) (56). RSEM v1.3.0 (57) was used to extract counts per gene. The counts per gene were normalized using Bioconductor package DESeq2 v1.14.1 (58). For further analysis, genes without at least one count in 10% of the organoids were discarded as well as genes not assigned as protein coding according to VEGA gene and transcript annotation from Ensembl human (release 91). An average of 50 million reads per sample were aligned to the reference genome.

Principal component analysis visualization

A principal component analysis (PCA) was performed on all organoids (normal and tumor organoids) using the normalized and filtered counts per gene (see RNA-seq analysis section). A variance stabilization transformation was performed using Bioconductor package DESeq2 v1.14.1 (58). The 2000 most variable genes were retained and used as input for the PCA analysis which was performed using R stats package (59). K-means clustering was performed on the PDO expression data reduced to three principle components, also using R stats package with the parameter for the number of clusters fixed to 2. The result of the PCA-based clustering was displayed using the CRAN package plotly v4.7.1 [https://CRAN.R-project.org/package=plotly].

Differential gene expression analysis normal vs tumor organoids

A differential gene expression (DGE) analysis was performed with Bioconductor package DESeq2 v1.14.1 (58) using the normalized and filtered counts per gene from the RNA-seq analysis. The DGE analysis was performed between normal and tumor organoids using DESeq2 likelihood ratio test (LRT).

Clustering of tumor organoids

Using only tumor organoids, a non-negative matrix factorization (NMF) clustering was performed on the 2000 most variable genes, as determined in the RNA-seq analysis, to identify stable tumor organoids clusters using CRAN package NMF v0.20.6 (60). The NMF parameters were: Brunet factorization method, rank of 2 through 7, 500 iterations. The best-performing clustering result was selected using the observed cophenetic correlation between clusters and the average silhouette width of the consensus matrices. The NMF clustering generated 2 stable tumor organoids clusters, labeled C1 and C2. Only the individuals with the higher consensus are included in C1 and C2 clusters. Three PDO cultures with poor cluster identity consensus were excluded from the subsequent differential expression analysis. The NMF clustering was refined to 245 genes (Figure 3, Table S3).

Differential gene expression analysis tumor organoids

A DGE analysis was performed on the tumor organoids only. A differential gene expression analysis was performed between C1 and C2 tumor organoids clusters using DESeq2 with default parameters. The CRAN package gplots v3.0.1 (https://CRAN.R-project.org/package=gplots) was used to generate a heatmap of the 250 genes most significantly differentially expressed between C1 and C2. Of these, 5 genes with a median expression count of zero were removed.

Pharmacotyping of organoids

Organoids were dissociated into single cells. 500 viable cells were plated per well in in 20μL 10% Matrigel / human complete organoid media. Therapeutic compounds were added 24 hours post plating, after the reformation of organoids was visually verified. Chemotherapeutic were tested in triplicates: gemcitabine, paclitaxel, SN38 range from $8.1x10^{-12}$ M to $2.0x10^{-6}$ M, and 5-FU and Oxaliplatin range from $1.0x10^{-8}$ M to $5.0x10^{-5}$ M. Targeted drugs were tested in singlicates (range from $1.0x10^{-8}$ M to $1.0x10^{-5}$ M). Compounds were dissolved in DMSO and all treatment wells were normalized to 0.5% DMSO content. After 5 days cell viability was assessed using CellTiter-Glo as per manufacturer's instruction (Promega) on a SpectraMax I3 (Molecular Devices) plate reader. A three-parameter log-logistic function with upper limit equal to the mean of the DMSO values was fit to the pharmacotyping data (viability vs. dose) with CRAN package drc v3.0-1 (61). Quality control was performed on the curve fitness: rejection of the curve if 100% plateau is located beyond 2 standard deviation of the mean DMSO control and visual inspection, leading to possible rejection, of the top 5% curves ranked with the highest sum of the squared differences between triplicate measurements and fitted curve. The area under the curve (AUC) was calculated using CRAN package Bolstad2 v1.0-28 (https://cran.r-project.org/web/packages/Bolstad2/). Normalized AUC was obtained by dividing the AUC value by the maximum area for the concentration range measured for each drug. The range of the normalized AUC is between 0 and 1.

Pharmacotranscriptomic analysis

For each drug, the Spearman's rank correlation coefficient was calculated between the organoid drug-specific AUC and the 10,000 most variably expressed genes (normalized counts) obtained from the RNA-seq analysis. The Spearman's rank correlation was selected to test for monotonic, but not necessarily linear, dependence between the AUC and the gene expression. For derivation of drug-specific transcriptional signatures, genes were filtered using the p-values for the Spearman's coefficient calculation as threshold (p-value < 0.01). Genes positively correlated with sensitivity ($r < -0.38$) to a chemotherapeutic drug were selected for validation in patient derived RNA-seq data (Table S5). Each filtered gene list was clustered separately using the Spearman's rank correlation coefficients. To rank sensitivity of PDOs and patients using RNA-seq data, mean z-score was computed for the individual drug sensitivity signature and ranked from high mean expression to low mean expression. A flow chart of the pharmacotranscriptomic analysis pipeline is presented in Figure S8.

Pathway analysis

Pathway analysis was performed with GSEA2 version 2.2.4 (62).

Supplementary Material

Refer to Web version on PubMed Central for supplementary material.

Authors

Hervé Tiriac[1], Pascal Belleau[1,33], Dannielle D. Engle[1,33], Dennis Plenker[1], Astrid Deschênes[1], Tim D. D. Somerville[1], Fieke E. M. Froeling[1], Richard A. Burkhart[2], Robert E. Denroche[3], Gun-Ho Jang[3], Koji Miyabayashi[1], C. Megan Young[1,4], Hardik Patel[1], Michelle Ma[1], Joseph F. LaComb[5], Randze Lerie D. Palmaira[6], Ammar A. Javed[2], Jasmine C. Huynh[7], Molly Johnson[8], Kanika Arora[8], Nicolas Robine[8], Minita Shah[8], Rashesh Sanghvi[8], Austin B. Goetz[9], Cinthya Y. Lowder[9], Laura Martello[10], Else Driehuis[11,12], Nicolas LeComte[6], Gokce Askan[6], Christine A. Iacobuzio-Donahue[6], Hans Clevers[11,12,13], Laura D. Wood[14], Ralph H. Hruban[14], Elizabeth Thompson[14], Andrew J. Aguirre[15], Brian M. Wolpin[15], Aaron Sasson[16], Joseph Kim[16], Maoxin Wu[17], Juan Carlos Bucobo[5], Peter Allen[6], Divyesh V. Sejpal[18], William Nealon[19], James D. Sullivan[19], Jordan M. Winter[9], Phyllis A. Gimotty[20], Jean L. Grem[21], Dominick J. DiMaio[22], Jonathan M. Buscaglia[5], Paul M. Grandgenett[23], Jonathan R. Brody[9], Michael A. Hollingsworth[23], Grainne M. O'Kane[24], Faiyaz Notta[3], Edward Kim[7], James M. Crawford[25], Craig Devoe[26], Allyson Ocean[27], Christopher L. Wolfgang[2], Kenneth H. Yu[6], Ellen Li[5], Christopher R. Vakoc[1], Benjamin Hubert[8], Sandra E. Fischer[28,29], Julie M. Wilson[3], Richard Moffitt[16,30], Jennifer Knox[24], Alexander Krasnitz[1], Steven Gallinger[3,24,31,32,*], and David A. Tuveson[1,*]

Affiliations

[1]Cold Spring Harbor Laboratory, Cold Spring Harbor, NY 11724 [2]Johns Hopkins University, Division of Hepatobiliary and Pancreatic Surgery, Baltimore, MD 21218 [3]PanCuRx Translational Research Initiative, Ontario Institute for Cancer Research, Toronto, Ontario Canada M5G 0A3 [4]Swiss Federal Institute of Technology Lausanne (EPFL), School of Life Sciences, Swiss Institute for Experimental Cancer Research (ISREC), Laboratory of Tumor Heterogeneity and Stemness in Cancer, Lausanne CH-1015, Switzerland [5]Stony Brook University, Department of Medicine, Stony Brook, NY 11794 [6]Memorial Sloan Kettering Cancer Center, New York, NY 10065 [7]University of California, Davis, Comprehensive Cancer Center, Division of Hematology and Oncology, Sacramento CA 95817 [8]New York Genome Center, New York, NY 10013 [9]Thomas Jefferson University, Department of Surgery, Philadelphia, PA 19107 [10]SUNY Downstate Medical Center, Department of Medicine, New York, NY 11203 [11]Hubrecht Institute, Royal Netherlands Academy of Arts and Sciences (KNAW), Utrecht, The Netherlands [12]University Medical Center (UMC), Utrecht, The Netherlands [13]Princess Maxime Center (PMC), Utrecht, The Netherlands [14]Johns Hopkins University, Department of Pathology, Baltimore, MD 21218 [15]Dana Farber Cancer Institute, Broad Institute, Boston, MA 02215 [16]Stony Brook University

Department of Surgery, Stony Brook, NY 11794 [17]Stony Brook University Department of Pathology, Stony Brook, NY 11794 [18]Donald and Barbara Zucker School of Medicine at Hofstra/Northwell, Division of Gastroenterology, Hempstead, NY, 11549 [19]Donald and Barbara Zucker School of Medicine at Hofstra/Northwell, Department of Surgery, Hempstead, NY, 11549 [20]University of Pennsylvania, Department of Biostatistics, Epidemiology and Informatics, Philadelphia, PA 19105 [21]University of Nebraska Medical Center, Department of Medicine, Omaha NE 68198 [22]University of Nebraska Medical Center, Department of Pathology and Microbiology, Omaha NE 68198 [23]University of Nebraska Medical Center, Eppley Institute for Research in Cancer and Allied Diseases, Fred & Pamela Buffet Cancer Center, Omaha NE 68198 [24]Wallace McCain Centre for Pancreatic Cancer, Department of Medical Oncology, Princess Margaret Cancer Centre, University Health Network, University of Toronto, Toronto, Ontario Canada M5G 2M9 [25]Donald and Barbara Zucker School of Medicine at Hofstra/Northwell, Department of Pathology and Laboratory Medicine, Hempstead, NY [26]Donald and Barbara Zucker School of Medicine at Hofstra/Northwell, Division of Medical Oncology, Hempstead, NY, 11549 [27]Weill Cornell Medical College, New York, NY 10021 [28]Department of Pathology, University Health Network, University of Toronto, Toronto, Ontario, Canada M5G 2C4 [29]Department of Laboratory Medicine and Pathobiology, University of Toronto, Toronto, Ontario, Canada M5G 2C4 [30]Stony Brook University: Department of Biomedical Informatics, Stony Brook, NY 11794 [31]Lunenfeld-Tanenbaum Research Institute, Mount Sinai Hospital, Toronto, Ontario, Canada M5G 1X5 [32]Hepatobiliary/Pancreatic Surgical Oncology Program, University Health Network, Toronto, Ontario, Canada M5G 2M9

Acknowledgments

We would like to thank the patients, families and clinicians that contributed to this work. This work was supported by the Lustgarten Foundation (D.A. Tuveson). D.A. Tuveson is a distinguished scholar of the Lustgarten Foundation and Director of the Lustgarten Foundation-Dedicated Laboratory of Pancreatic Cancer Research. S.Gallinger is supported by the Ontario Institute for Cancer Research, a, charitable donations from the Canadian Friends of the Hebrew University (Alex U. Soyka) and the Pancreatic Cancer Canada Foundation, and the Lebovich Chair in Hepatobiliary/Pancreatic Surgical Oncology. This project was also supported in part by the NCI/LEIDOS Human Cancer Models Initiative (HHSN26100008) (D.A. Tuveson, H. Clevers, J.M. Crawford), National Institutes of Health 5P50CA101955-07 (D.A. Tuveson), P20CA192996-03 (D.A. Tuveson), 1U10CA180944-04 (D.A. Tuveson), 5U01CA168409-5 (D.A. Tuveson), 1R01CA188134-01 (D.A. Tuveson), 1R01CA190092-04 (D.A. Tuveson), 5T32CA148056 (D.D. Engle), 5K99CA204725 (D.D. Engle), 5P01CA013106 (C.R. Vakoc), 5P30CA45508 (D.A. Tuveson, P.A. Gilmoty), 1R01CA212600-01 (J.R. Brody, J.M. Winter), P20CA192994 (E. Li), R01CA202762 (K.H. Yu), P50CA127297 (M. A. Hollingsworth, UNMC RAP), U01CA210240 (M. A. Hollingsworth, D.A. Tuveson, UNMC RAP), and 5R50CA211462 (M. A. Hollingsworth, UNMC RAP), V Foundation Translational Grant (K.H. Yu and D.A. Tuveson), Cold Spring Harbor Laboratory Association (D.A. Tuveson), Stand Up to Cancer/AACRPS09 (D.A. Tuveson), Precision Medicine Research Associates (D.A. Tuveson), SWOG ITSC 5U10CA180944-04 (D.A. Tuveson, H. Tiriac, E.J. Kim), Pancreatic Cancer Action Network-AACR 16-20-25-VAKO (C.R.Vakoc), State of New York C150158 (T.D.D. Somerville – The Opinions, results, findings and/or interpretation of data contained herein are the responsibility of the authors and do not necessarily represent the opinions, interpretations or policy of New York State), Concetta Greenberg in memory of Marvin S. Greenberg, M.D (J.R. Brody, J.M. Winter), RAN grant from the AACR Pancreatic Cancer Action Network (J.R. Brody, J.M. Winter), ASGE Endoscopic Research Award 71040 (J.M. Buscaglia), Simons Foundation Award 415604 (E. Li), Canadian Cancer Society Research Institute grant 702316 (S. Gallinger). We acknowledge the Cold Spring Harbor Laboratory Tissue Culture and Next Generation Sequencing Shared Resources, which are funded by the NIH Cancer Center Support Grant 5P30CA045508. We also acknowledge the contributions of Production Sequencing, Genome Sequencing Informatics and Tissue Portal (Diagnostic

Development) at the Ontario Institute for Cancer Research, as well as the University Health Network BioBank. The pancreatic cancer patient study (ICGC-CA, COMPASS) was conducted with the support of the Ontario Institute for Cancer Research (PanCuRx Translational Research Initiative) through funding provided by the Government of Ontario.

References

1. Khorana AA, Mangu PB, Berlin J, Engebretson A, Hong TS, Maitra A, et al. Potentially Curable Pancreatic Cancer: American Society of Clinical Oncology Clinical Practice Guideline. J Clin Oncol. 2016; 34:2541–56. [PubMed: 27247221]
2. Winter JM, Cameron JL, Campbell KA, Arnold MA, Chang DC, Coleman J, et al. 1423 pancreaticoduodenectomies for pancreatic cancer: A single-institution experience. J Gastrointest Surg. 2006; 10:1199–210. discussion 210-1. [PubMed: 17114007]
3. Groot VP, Rezaee N, Wu W, Cameron JL, Fishman EK, Hruban RH, et al. Patterns, Timing, and Predictors of Recurrence Following Pancreatectomy for Pancreatic Ductal Adenocarcinoma. Ann Surg. 2017
4. Neoptolemos JP, Palmer DH, Ghaneh P, Psarelli EE, Valle JW, Halloran CM, et al. Comparison of adjuvant gemcitabine and capecitabine with gemcitabine monotherapy in patients with resected pancreatic cancer (ESPAC-4): a multicentre, open-label, randomised, phase 3 trial. Lancet. 2017; 389:1011–24. [PubMed: 28129987]
5. Sinn M, Bahra M, Liersch T, Gellert K, Messmann H, Bechstein W, et al. CONKO-005: Adjuvant Chemotherapy With Gemcitabine Plus Erlotinib Versus Gemcitabine Alone in Patients After R0 Resection of Pancreatic Cancer: A Multicenter Randomized Phase III Trial. J Clin Oncol. 2017; 35:3330–7. [PubMed: 28817370]
6. Von Hoff DD, Ervin T, Arena FP, Chiorean EG, Infante J, Moore M, et al. Increased survival in pancreatic cancer with nab-paclitaxel plus gemcitabine. N Engl J Med. 2013; 369:1691–703. [PubMed: 24131140]
7. Conroy T, Desseigne F, Ychou M, Bouche O, Guimbaud R, Becouarn Y, et al. FOLFIRINOX versus gemcitabine for metastatic pancreatic cancer. N Engl J Med. 2011; 364:1817–25. [PubMed: 21561347]
8. Le DT, Durham JN, Smith KN, Wang H, Bartlett BR, Aulakh LK, et al. Mismatch repair deficiency predicts response of solid tumors to PD-1 blockade. Science. 2017; 357:409–13. [PubMed: 28596308]
9. Waddell N, Pajic M, Patch AM, Chang DK, Kassahn KS, Bailey P, et al. Whole genomes redefine the mutational landscape of pancreatic cancer. Nature. 2015; 518:495–501. [PubMed: 25719666]
10. Ostrem JM, Peters U, Sos ML, Wells JA, Shokat KM. K-Ras(G12C) inhibitors allosterically control GTP affinity and effector interactions. Nature. 2013; 503:548–51. [PubMed: 24256730]
11. Bailey P, Chang DK, Nones K, Johns AL, Patch AM, Gingras MC, et al. Genomic analyses identify molecular subtypes of pancreatic cancer. Nature. 2016; 531:47–52. [PubMed: 26909576]
12. Collisson EA, Sadanandam A, Olson P, Gibb WJ, Truitt M, Gu S, et al. Subtypes of pancreatic ductal adenocarcinoma and their differing responses to therapy. Nat Med. 2011; 17:500–3. [PubMed: 21460848]
13. Moffitt RA, Marayati R, Flate EL, Volmar KE, Loeza SG, Hoadley KA, et al. Virtual microdissection identifies distinct tumor- and stroma-specific subtypes of pancreatic ductal adenocarcinoma. Nat Genet. 2015; 47:1168–78. [PubMed: 26343385]
14. Cancer Genome Atlas Research Network. Integrated Genomic Characterization of Pancreatic Ductal Adenocarcinoma. Cancer Cell. 2017; 32:185–203 e13. [PubMed: 28810144]
15. Boj SF, Hwang CI, Baker LA, Chio II, Engle DD, Corbo V, et al. Organoid models of human and mouse ductal pancreatic cancer. Cell. 2015; 160:324–38. [PubMed: 25557080]
16. Tiriac H, Bucobo JC, Tzimas D, Grewel S, Lacomb JF, Rowehl LM, et al. Successful creation of pancreatic cancer organoids by means of EUS-guided fine-needle biopsy sampling for personalized cancer treatment. Gastrointest Endosc. 2018
17. Seino T, Kawasaki S, Shimokawa M, Tamagawa H, Toshimitsu K, Fujii M, et al. Human Pancreatic Tumor Organoids Reveal Loss of Stem Cell Niche Factor Dependence during Disease Progression. Cell Stem Cell. 2018; 22:454–67 e6. [PubMed: 29337182]

18. Zhang Y, Kwok-Shing Ng P, Kucherlapati M, Chen F, Liu Y, Tsang YH, et al. A Pan-Cancer Proteogenomic Atlas of PI3K/AKT/mTOR Pathway Alterations. Cancer Cell. 2017; 31:820–32 e3. [PubMed: 28528867]
19. Diamond EL, Durham BH, Haroche J, Yao Z, Ma J, Parikh SA, et al. Diverse and Targetable Kinase Alterations Drive Histiocytic Neoplasms. Cancer Discov. 2016; 6:154–65. [PubMed: 26566875]
20. Donovan KF, Hegde M, Sullender M, Vaimberg EW, Johannessen CM, Root DE, et al. Creation of Novel Protein Variants with CRISPR/Cas9-Mediated Mutagenesis: Turning a Screening By-Product into a Discovery Tool. PLoS One. 2017; 12:e0170445. [PubMed: 28118392]
21. Greulich H, Kaplan B, Mertins P, Chen TH, Tanaka KE, Yun CH, et al. Functional analysis of receptor tyrosine kinase mutations in lung cancer identifies oncogenic extracellular domain mutations of ERBB2. Proc Natl Acad Sci U S A. 2012; 109:14476–81. [PubMed: 22908275]
22. Pritchard CC, Smith C, Salipante SJ, Lee MK, Thornton AM, Nord AS, et al. ColoSeq Provides Comprehensive Lynch and Polyposis Syndrome Mutational Analysis Using Massively Parallel Sequencing. The Journal of Molecular Diagnostics. 14:357–66.
23. Wolff RA, Wang-Gillam A, Alvarez H, Tiriac H, Engle D, Hou S, et al. Dynamic changes during the treatment of pancreatic cancer. Oncotarget. 2018; 9:14764–90. [PubMed: 29599906]
24. Beuvink I, Boulay A, Fumagalli S, Zilbermann F, Ruetz S, O'Reilly T, et al. The mTOR inhibitor RAD001 sensitizes tumor cells to DNA-damaged induced apoptosis through inhibition of p21 translation. Cell. 2005; 120:747–59. [PubMed: 15797377]
25. Connor AA, Denroche RE, Jang GH, Timms L, Kalimuthu SN, Selander I, et al. Association of Distinct Mutational Signatures With Correlates of Increased Immune Activity in Pancreatic Ductal Adenocarcinoma. JAMA Oncol. 2017; 3:774–83. [PubMed: 27768182]
26. Aung KL, Fischer SE, Denroche RE, Jang G-H, Dodd A, Creighton S, et al. Genomics-Driven Precision Medicine for Advanced Pancreatic Cancer: Early Results from the COMPASS Trial. Clinical Cancer Research. 2018; 24:1344. [PubMed: 29288237]
27. Chio IIC, Jafarnejad SM, Ponz-Sarvise M, Park Y, Rivera K, Palm W, et al. NRF2 Promotes Tumor Maintenance by Modulating mRNA Translation in Pancreatic Cancer. Cell. 166:963–76.
28. Biancur DE, Paulo JA, Małachowska B, Quiles Del Rey M, Sousa CM, Wang X, et al. Compensatory metabolic networks in pancreatic cancers upon perturbation of glutamine metabolism. Nature Communications. 2017; 8:15965.
29. Commisso C, Davidson SM, Soydaner-Azeloglu RG, Parker SJ, Kamphorst JJ, Hackett S, et al. Macropinocytosis of protein is an amino acid supply route in Ras-transformed cells. Nature. 2013; 497:633. [PubMed: 23665962]
30. Jacobetz MA, Chan DS, Neesse A, Bapiro TE, Cook N, Frese KK, et al. Hyaluronan impairs vascular function and drug delivery in a mouse model of pancreatic cancer. Gut. 2013; 62:112–20. [PubMed: 22466618]
31. Olive KP, Jacobetz MA, Davidson CJ, Gopinathan A, McIntyre D, Honess D, et al. Inhibition of Hedgehog signaling enhances delivery of chemotherapy in a mouse model of pancreatic cancer. Science. 2009; 324:1457–61. [PubMed: 19460966]
32. Provenzano PP, Cuevas C, Chang AE, Goel VK, Von Hoff DD, Hingorani SR. Enzymatic targeting of the stroma ablates physical barriers to treatment of pancreatic ductal adenocarcinoma. Cancer Cell. 2012; 21:418–29. [PubMed: 22439937]
33. Balli D, Rech AJ, Stanger BZ, Vonderheide RH. Immune Cytolytic Activity Stratifies Molecular Subsets of Human Pancreatic Cancer. Clinical Cancer Research. 2017; 23:3129. [PubMed: 28007776]
34. Geller LT, Barzily-Rokni M, Danino T, Jonas OH, Shental N, Nejman D, et al. Potential role of intratumor bacteria in mediating tumor resistance to the chemotherapeutic drug gemcitabine. Science. 2017; 357:1156–60. [PubMed: 28912244]
35. Hessmann E, Patzak MS, Klein L, Chen N, Kari V, Ramu I, et al. Fibroblast drug scavenging increases intratumoural gemcitabine accumulation in murine pancreas cancer. Gut. 2018; 67:497. [PubMed: 28077438]

36. Mihara E, Hirai H, Yamamoto H, Tamura-Kawakami K, Matano M, Kikuchi A, et al. Active and water-soluble form of lipidated Wnt protein is maintained by a serum glycoprotein afamin/alpha-albumin. Elife. 2016:5.
37. Li H, Durbin R. Fast and accurate short read alignment with Burrows-Wheeler transform. Bioinformatics. 2009; 25:1754–60. [PubMed: 19451168]
38. McKenna A, Hanna M, Banks E, Sivachenko A, Cibulskis K, Kernytsky A, et al. The Genome Analysis Toolkit: a MapReduce framework for analyzing next-generation DNA sequencing data. Genome Res. 2010; 20:1297–303. [PubMed: 20644199]
39. Cibulskis K, Lawrence MS, Carter SL, Sivachenko A, Jaffe D, Sougnez C, et al. Sensitive detection of somatic point mutations in impure and heterogeneous cancer samples. Nat Biotechnol. 2013; 31:213–9. [PubMed: 23396013]
40. Wilm A, Aw PP, Bertrand D, Yeo GH, Ong SH, Wong CH, et al. LoFreq: a sequence-quality aware, ultra-sensitive variant caller for uncovering cell-population heterogeneity from high-throughput sequencing datasets. Nucleic Acids Res. 2012; 40:11189–201. [PubMed: 23066108]
41. Saunders CT, Wong WS, Swamy S, Becq J, Murray LJ, Cheetham RK. Strelka: accurate somatic small-variant calling from sequenced tumor-normal sample pairs. Bioinformatics. 2012; 28:1811–7. [PubMed: 22581179]
42. Ye K, Schulz MH, Long Q, Apweiler R, Ning Z. Pindel: a pattern growth approach to detect break points of large deletions and medium sized insertions from paired-end short reads. Bioinformatics. 2009; 25:2865–71. [PubMed: 19561018]
43. Narzisi G, O'Rawe JA, Iossifov I, Fang H, Lee YH, Wang Z, et al. Accurate de novo and transmitted indel detection in exome-capture data using microassembly. Nat Methods. 2014; 11:1033–6. [PubMed: 25128977]
44. Wang J, Mullighan CG, Easton J, Roberts S, Heatley SL, Ma J, et al. CREST maps somatic structural variation in cancer genomes with base-pair resolution. Nat Methods. 2011; 8:652–4. [PubMed: 21666668]
45. Rausch T, Zichner T, Schlattl A, Stutz AM, Benes V, Korbel JO. DELLY: structural variant discovery by integrated paired-end and split-read analysis. Bioinformatics. 2012; 28:i333–i9. [PubMed: 22962449]
46. Chen K, Wallis JW, McLellan MD, Larson DE, Kalicki JM, Pohl CS, et al. BreakDancer: an algorithm for high-resolution mapping of genomic structural variation. Nat Methods. 2009; 6:677–81. [PubMed: 19668202]
47. Xi R, Lee S, Xia Y, Kim TM, Park PJ. Copy number analysis of whole-genome data using BIC-seq2 and its application to detection of cancer susceptibility variants. Nucleic Acids Res. 2016; 44:6274–86. [PubMed: 27260798]
48. Shen R, Seshan VE. FACETS: allele-specific copy number and clonal heterogeneity analysis tool for high-throughput DNA sequencing. Nucleic Acids Res. 2016; 44:e131. [PubMed: 27270079]
49. Ha G, Roth A, Khattra J, Ho J, Yap D, Prentice LM, et al. TITAN: inference of copy number architectures in clonal cell populations from tumor whole-genome sequence data. Genome Res. 2014; 24:1881–93. [PubMed: 25060187]
50. Carter SL, Cibulskis K, Helman E, McKenna A, Shen H, Zack T, et al. Absolute quantification of somatic DNA alterations in human cancer. Nat Biotechnol. 2012; 30:413–21. [PubMed: 22544022]
51. Skidmore ZL, Wagner AH, Lesurf R, Campbell KM, Kunisaki J, Griffith OL, et al. GenVisR: Genomic Visualizations in R. Bioinformatics. 2016; 32:3012–4. [PubMed: 27288499]
52. Gu Z, Eils R, Schlesner M. Complex heatmaps reveal patterns and correlations in multidimensional genomic data. Bioinformatics. 2016; 32:2847–9. [PubMed: 27207943]
53. Gu Z, Eils R, Schlesner M. gtrellis: an R/Bioconductor package for making genome-level Trellis graphics. BMC Bioinformatics. 2016; 17:169. [PubMed: 27089965]
54. Bolger AM, Lohse M, Usadel B. Trimmomatic: a flexible trimmer for Illumina sequence data. Bioinformatics. 2014; 30:2114–20. [PubMed: 24695404]
55. Dobin A, Davis CA, Schlesinger F, Drenkow J, Zaleski C, Jha S, et al. STAR: ultrafast universal RNA-seq aligner. Bioinformatics. 2013; 29:15–21. [PubMed: 23104886]

56. Harrow J, Frankish A, Gonzalez JM, Tapanari E, Diekhans M, Kokocinski F, et al. GENCODE: the reference human genome annotation for The ENCODE Project. Genome Res. 2012; 22:1760–74. [PubMed: 22955987]

57. Li B, Dewey CN. RSEM: accurate transcript quantification from RNA-Seq data with or without a reference genome. BMC Bioinformatics. 2011; 12:323. [PubMed: 21816040]

58. Love MI, Huber W, Anders S. Moderated estimation of fold change and dispersion for RNA-seq data with DESeq2. Genome Biol. 2014; 15:550. [PubMed: 25516281]

59. Team RC. R: A language and environment for statistical computing. R Foundation for Statistical Computing; 2014.

60. Gaujoux R, Seoighe C. A flexible R package for nonnegative matrix factorization. BMC Bioinformatics. 2010; 11:367. [PubMed: 20598126]

61. Ritz C, Baty F, Streibig JC, Gerhard D. Dose-Response Analysis Using R. PLoS One. 2015; 10:e0146021. [PubMed: 26717316]

62. Subramanian A, Tamayo P, Mootha VK, Mukherjee S, Ebert BL, Gillette MA, et al. Gene set enrichment analysis: A knowledge-based approach for interpreting genome-wide expression profiles. Proceedings of the National Academy of Sciences of the United States of America. 2005; 102:15545–50. [PubMed: 16199517]

Statement of significance

New approaches to prioritize treatment strategies are urgently needed to improve survival and quality of life for pancreatic cancer patients. Combined genomic, transcriptomic, and therapeutic profiling of patient-derived organoids can identify molecular and functional subtypes of pancreatic cancer, predict therapeutic responses and facilitate precision medicine for pancreatic cancer patients.

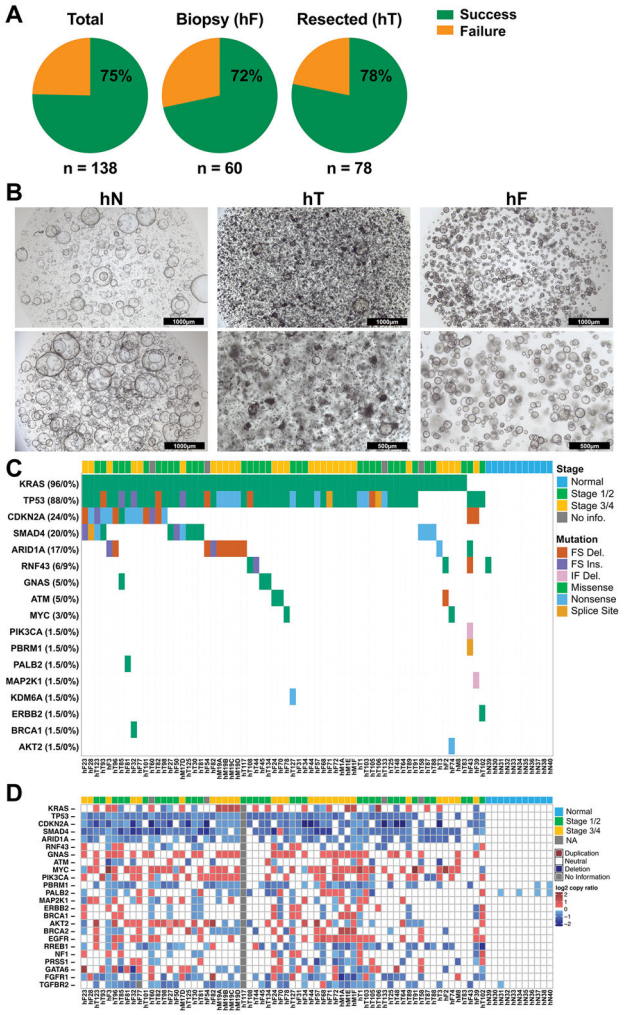

Figure 1. Genomic landscape of pancreatic cancer PDO

A. Isolation efficiency rate of PDOs from total samples, biopsies (hF), and resected surgical specimens (hT). **B**. PDO morphology in brightfield microscopy. Scale bars are 1000 or 500 μm as indicated. **C.** Single nucleotide variants in the PDO library. Mutation frequency indicated in both cancer and normal organoids (cancer % (left) / normal % (right)). Only mutations reported in COSMIC were included. Patient staging and type of mutation are denoted by a color-coded key. FS = Frameshift, Del. = Deletion, Ins. = Insertion, IF = In Frame, NA = Not Available. **D**. Copy number alterations (−2.0 through −0.235 and 0.235 through 2.0 $\log_2$ copy number ratio color key) in the PDO library. The cancer stages of the patients are indicated.

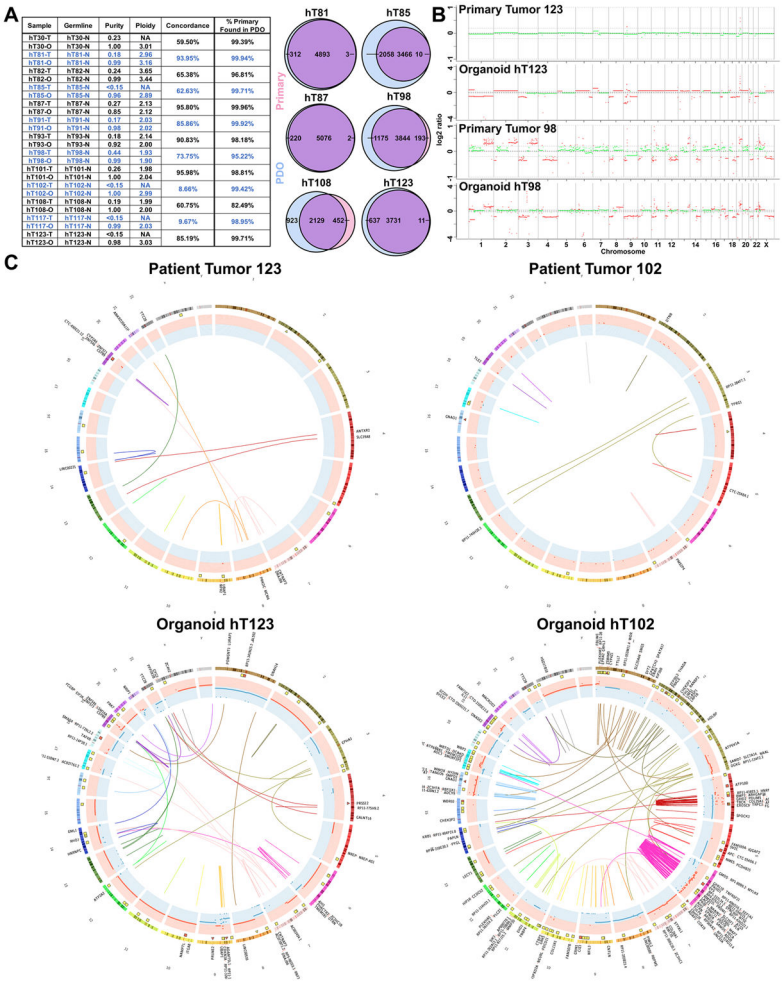

Sample	Germline	Purity	Ploidy	Concordance	% Primary Found in PDO
hT30-T	hT30-N	0.23	NA	59.50%	99.39%
hT30-O	hT30-N	1.00	3.01		
hT81-T	hT81-N	0.18	2.86	93.95%	99.94%
hT81-O	hT81-N	0.99	3.16		
hT82-T	hT82-N	0.24	3.65	65.38%	96.81%
hT82-O	hT82-N	0.99	3.44		
hT85-T	hT85-N	<0.15	NA	62.63%	99.71%
hT85-O	hT85-N	0.96	2.89		
hT87-T	hT87-N	0.27	2.13	95.80%	99.96%
hT87-O	hT87-N	0.85	2.12		
hT91-T	hT91-N	0.17	2.03	85.86%	99.92%
hT91-O	hT91-N	0.98	2.02		
hT93-T	hT93-N	0.18	2.14	90.83%	98.18%
hT93-O	hT93-N	0.92	2.00		
hT98-T	hT98-N	0.44	1.93	73.75%	95.22%
hT98-O	hT98-N	0.99	1.90		
hT101-T	hT101-N	0.26	1.98	95.98%	98.81%
hT101-O	hT101-N	1.00	2.04		
hT102-T	hT102-N	<0.15	NA	8.66%	99.42%
hT102-O	hT102-N	1.00	2.99		
hT108-T	hT108-N	0.19	1.99	60.75%	82.49%
hT108-O	hT108-N	1.00	2.00		
hT117-T	hT117-N	<0.15	NA	9.67%	98.95%
hT117-O	hT117-N	0.99	2.03		
hT123-T	hT123-N	<0.15	NA	85.19%	99.71%
hT123-O	hT123-N	0.98	3.03		

Figure 2. Deep molecular clarity obtained from PDO genetic analyses

A. Purity, ploidy, concordance and percent of the primary tumor mutations found in the PDO cultures using whole genome SNVs of the PDO and matched primary tumor specimens following germline variant removal. Representative Venn diagrams are shown of PDO and Primary Tumor SNVs. **B**. CNA in representative matched primary tumor specimens and corresponding PDO. Two representative cases with differing degrees of primary tumor purity are shown. **C.** Circos plots demonstrating CNA (red and blue CNA inner circles) and gross chromosomal rearrangements (connecting lines) in representative, matched primary tumor and PDOs following germline variant removal.

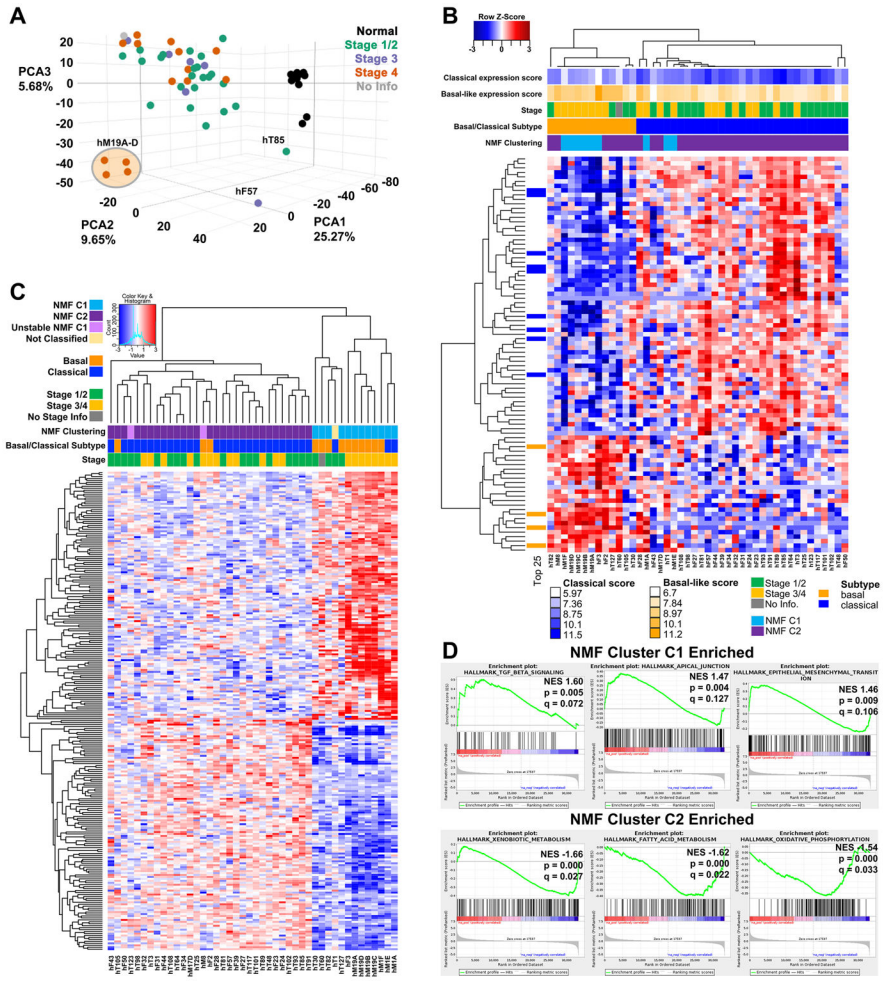

Figure 3. Transcriptomic profiling of PDOs reveals distinct subtypes

A. Principal component analysis of organoids isolated from different cancer stages and normal healthy controls. **B** Clustering of PDO culture RNA-seq data reveals concordance with Classical and Basal-like subtypes. Patient staging and subtype are indicated. **C**. Clustering using Non-negative Matrix Factorization defines two distinct clusters of PDO cultures, C1 and C2. Patient staging and subtype are indicated. **D**. GSEA of genes differentially expressed genes between C1 and C2. Three Hallmark pathways are shown to be enriched in C1 compared to C2 (top panels), and three are enriched in C2 (lower panels, negative enrichment C1/C2).

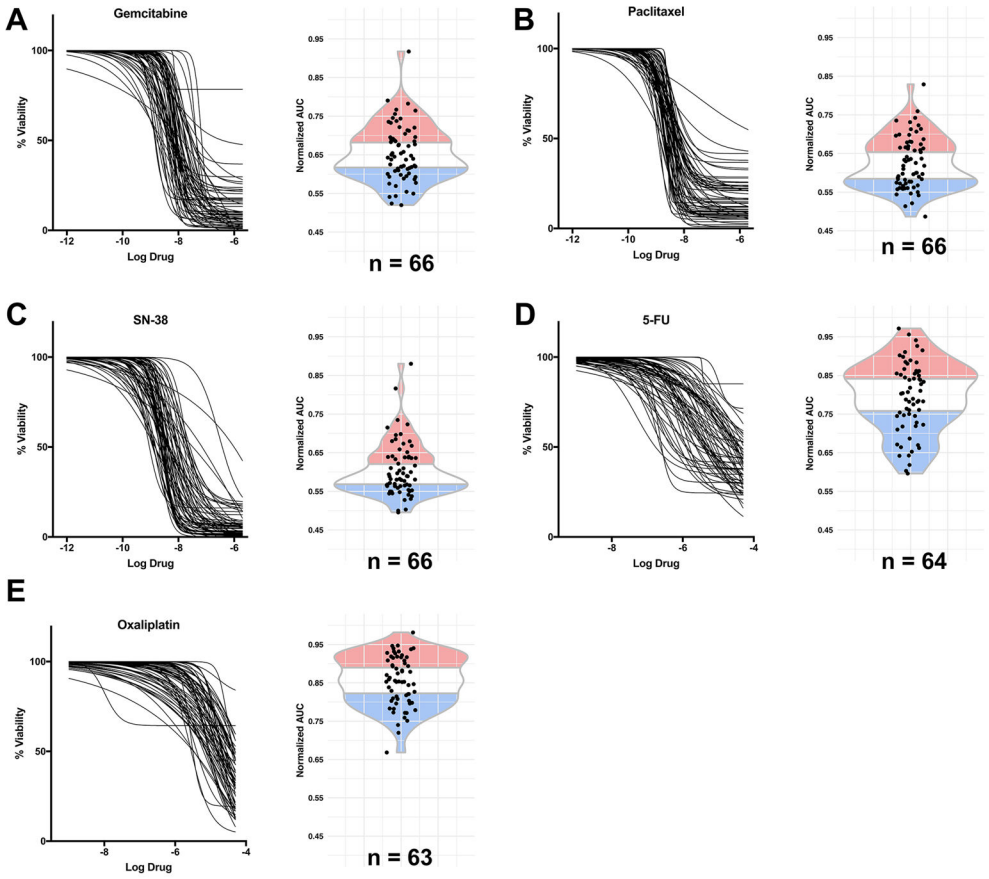

Figure 4. Pharmacotyping of PDOs reveals heterogeneity of chemotherapy response

A–E: Dose-response curves and normalized AUC distribution for Gemcitabine (**A**), Paclitaxel (**B**), SN-38 (**C**), 5-FU (**D**), and Oxaliplatin (**E**) on PDO cultures (n = 63 – 66). The blue portion represents the 33% most sensitive samples, the red portion the 34% most resistant samples, and the middle portion intermediate drug responses.

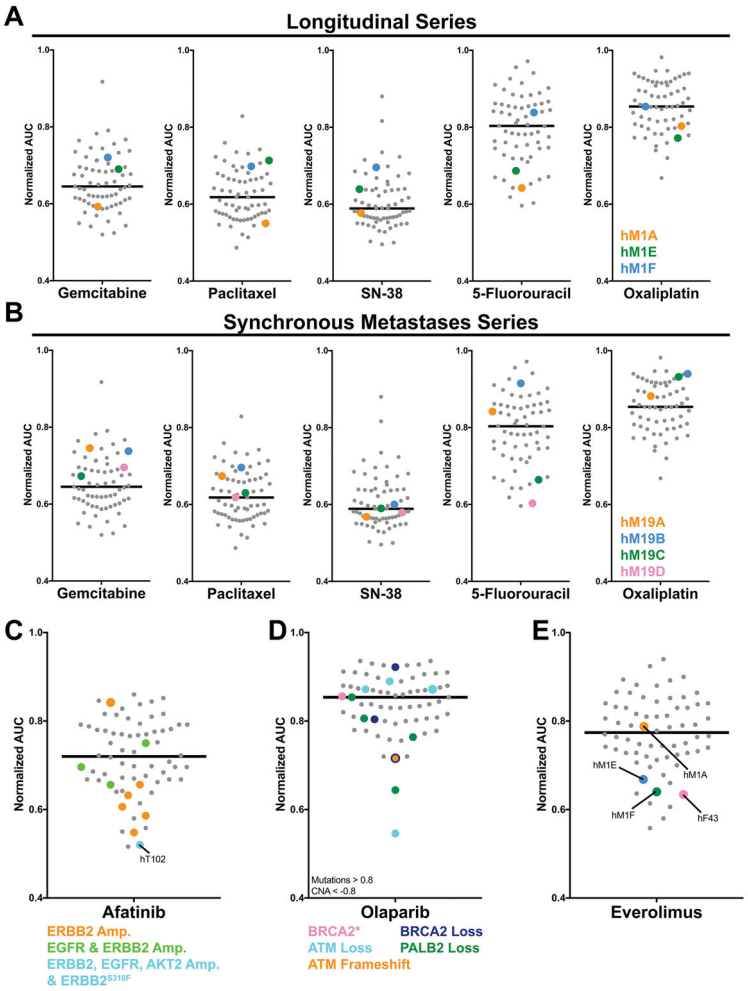

Figure 5. Longitudinal, spatial and genetic influences on PDO response

A. AUC distribution of hM1A, E and F PDO longitudinal series. **B**. AUC distribution of hM19 A, B, C, and D PDOs from the same patient but different metastatic sites. **C–E.** AUC distribution and genotype correlation of Afatinib (**C**), Olaparib (**D**), and Everolimus (**E**) responders.

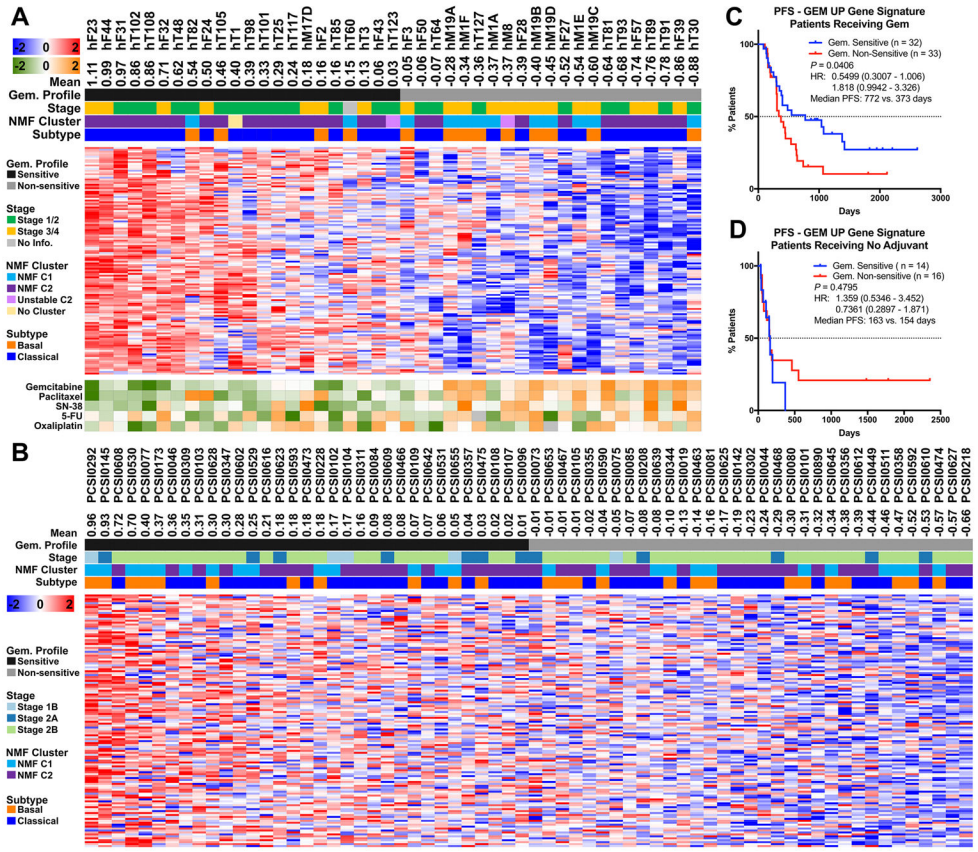

Figure 6. PDO-derived Gemcitabine sensitivity signature stratifies pancreatic cancer patients with improved response to adjuvant Gemcitabine

A. The Gemcitabine sensitivity prediction signature was used to cluster the PDO RNA-seq data. Additional data regarding the Pharmacotyping AUC response (log_2 transformed z-score), C1/C2 subtype, Basal/Classical subtype, and stage are shown. **B**. The Gemcitabine sensitivity prediction signature was applied to RNA-seq data from patients who received single-agent Gemcitabine (ICGC-CA). Additional data regarding the Pharmacotyping AUC response (log_2 transformed z-score), C1/C2 subtype, Basal/Classical subtype, and stage are shown. **C**. Kaplan-Meier analysis of PFS of Gemcitabine-sensitive and non-sensitive patients as identified in **B. D.** Kaplan-Meier analysis of PFS of Gemcitabine-sensitive and non-sensitive untreated patients. Log-rank (Mantel-Cox) test P value and log-rank Hazard Ratio are shown.

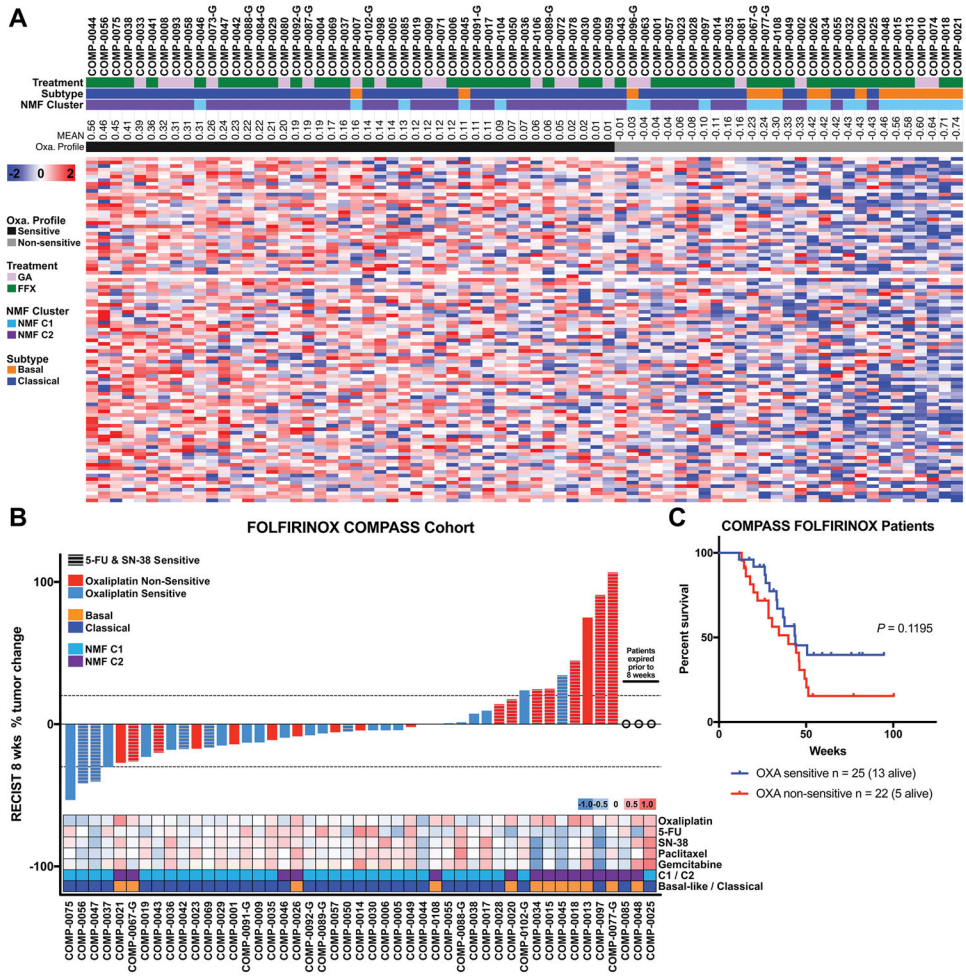

Figure 7. PDO-derived Oxaliplatin sensitivity signature stratifies advanced pancreatic cancer patients with improved response to FOLFIRINOX

A. The PDO-derived sensitivity signatures were applied to the RNA-seq data from 73 patients enrolled on the COMPASS trial that received either m-FOLFIRINOX or Gemcitabine with nab-Paclitaxel. **B.** A waterfall plot of the patients with RECIST criteria at 8 weeks post baseline that received FOLFIRINOX. Oxaliplatin signature significantly correlated with response (r = −0.396, P = 0.0078). Additional data regarding the mean chemotherapeutic signature scores, C1/C2 subtype, and Basal/Classical subtype are shown. **C.** The overall survival of patients receiving m-FOLFIRINOX segregated by their enrichment of the Oxaliplatin signature. Log-rank (Mantel-Cox) test P value.